

PAPER • OPEN ACCESS

Impact of skull sutures, spongiform bone distribution, and aging skull conductivities on the EEG forward and inverse problems

To cite this article: Hannah McCann and Leandro Beltrachini 2022 *J. Neural Eng.* **19** 016014

View the [article online](#) for updates and enhancements.

You may also like

- [Molecular genetics of craniosynostosis](#)
Caterine and Elza Ibrahim Auerkari
- [Exploring platelet lysate hydrogel-coated suture threads as biofunctional composite living fibers for cell delivery in tissue repair](#)
Raquel Costa-Almeida, Isabel Calejo, Roberta Altieri et al.
- [Smart self-tightening surgical suture from a tough bio-based hyperbranched polyurethane/reduced carbon dot nanocomposite](#)
Ritupama Duarah, Yogendra P Singh, Prerak Gupta et al.



PAPER

OPEN ACCESS

RECEIVED
14 September 2021

REVISED
8 December 2021

ACCEPTED FOR PUBLICATION
16 December 2021

PUBLISHED
1 February 2022

Original content from
this work may be used
under the terms of the
[Creative Commons
Attribution 4.0 licence](#).

Any further distribution
of this work must
maintain attribution to
the author(s) and the title
of the work, journal
citation and DOI.



Impact of skull sutures, spongiform bone distribution, and aging skull conductivities on the EEG forward and inverse problems

Hannah McCann^{1,2,*} and Leandro Beltrachini^{1,2}

¹ School of Physics and Astronomy, Cardiff University, Cardiff, United Kingdom

² Cardiff University Brain Research Imaging Centre (CUBRIC), Cardiff, United Kingdom

* Author to whom any correspondence should be addressed.

E-mail: mccannhm@cardiff.ac.uk

Keywords: forward problem, skull conductivity, inverse problem, electroencephalography, skull sutures

Supplementary material for this article is available [online](#)

Abstract

Objective. Source imaging is a principal objective for electroencephalography (EEG), the solutions of which require forward problem (FP) computations characterising the electric potential distribution on the scalp due to known sources. Additionally, the EEG-FP is dependent upon realistic, anatomically correct volume conductors and accurate tissue conductivities, where the skull is particularly important. Skull conductivity, however, deviates according to bone composition and the presence of adult sutures. The presented study therefore analyses the effect the presence of adult sutures and differing bone composition have on the EEG-FP and inverse problem (IP) solutions. **Approach.** Utilising a well-established head atlas, detailed head models were generated including compact and spongiform bone and adult sutures. The true skull conductivity was considered as inhomogeneous according to spongiform bone proportion and sutures. The EEG-FP and EEG-IP were solved and compared to results employing homogeneous skull models, with varying conductivities and omitting sutures, as well as using a hypothesised aging skull conductivity model. **Main results.** Significant localised FP errors, with relative error up to 85%, were revealed, particularly evident along suture lines and directly related to the proportion of spongiform bone. This remained evident at various ages. Similar EEG-IP inaccuracies were found, with the largest (maximum 4.14 cm) across suture lines. **Significance.** It is concluded that modelling the skull as an inhomogeneous layer that varies according to spongiform bone proportion and includes differing suture conductivity is imperative for accurate EEG-FP and source localisation calculations. Their omission can result in significant errors, relevant for EEG research and clinical diagnosis.

1. Introduction

Electroencephalography (EEG) is a non-invasive imaging modality used for characterising the electrical activity of the brain (Henry 2006). Localising the source of such activity provides valuable information for understanding brain function in health and disease, as well as aiding in the diagnosis of neurological disorders and syndromes such as epilepsy (Michel *et al* 2004) and attention deficit hyperactivity disorder (Ibáñez *et al* 2011). Source analysis involves, in a first instance, the characterisation of the current propagation from a known endogenous source to the scalp, known as the EEG forward problem (EEG-FP). The signal origin can then be estimated

from the recorded data and personalised FP computations, a process referred to as the EEG inverse problem (EEG-IP) (Haueisen *et al* 1999). Accurate solutions to these problems require the adoption of realistic and individualised volume conductor models incorporating precise anatomical tissues' geometries and their electrical conductivities. Within all tissue compartments, the skull has been pointed as the most relevant for EEG signal analysis, mostly due to its high resistivity (Gençer and Acar 2004, Dannhaeur *et al* 2011, McCann *et al* 2019, Vorwerk *et al* 2019). Although the majority of current studies incorporate realistic geometries from complementary medical images, the conductivities of all tissues, including the skull, are typically assumed from existing literature.

This poses a limitation to model personalisation as it is now accepted that most tissues, and in particular the skull, are subject to large variability between participants and measurement methods and protocols (McCann *et al* 2019). Misspecification of this conductivity, when considered as one compartment, has resulted in significant EEG forward and inverse solution errors (Vallaghé *et al* 2008, Chen *et al* 2010, Acar *et al* 2013, Vorwerk *et al* 2019). Incorporating accurate skull conductivity volumes is therefore imperative for the most precise resolution to the EEG FP and IP.

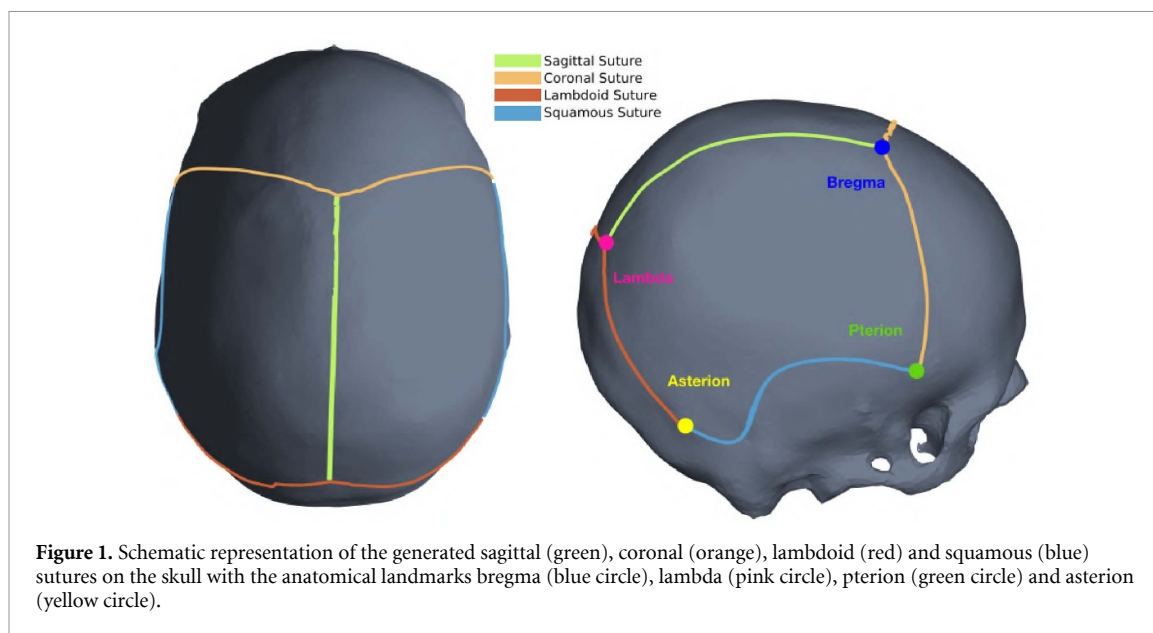
The skull, however, is geometrically complex and its simplification into one homogeneous layer is insufficient for accurate EEG source localisation (Dannhauer *et al* 2011). Within the field, the skull is accepted to be composed of three layers: a diploë (spongiform/marrow bone) layer, sandwiched between two compact (hard bone) compartments that are less conductive than the former (Tang *et al* 2008, McCann *et al* 2019). The percentage of bone marrow varies throughout the skull depending on overall skull thickness and location, leading to an inhomogeneous conductivity profile (Law 1993, Tang *et al* 2008). Accounting for the varying presence of spongiform and compact bone is essential, which can be only done in detail by means of computed tomography (CT) (Fernández-Corazza *et al* 2017) or unconventional magnetic resonance imaging (MRI) (Antonakakis *et al* 2020). Previous research has indicated that neglecting such detailed segmentation and assuming the skull as one homogeneous conductivity layer can result in EEG inverse solution errors of up to 2 cm (Wolters *et al* 2006, Dannhauer *et al* 2011, Montes *et al* 2011, Lanfer *et al* 2012, Montes-Restrepo *et al* 2014).

Although inhomogeneous skull models accounting for both spongiform and compact bone are increasingly employed, adult sutures are omitted, mainly due to the necessity of CT data and uncertainty regarding their impact. The sutures are dense, fibrous, immovable joints mostly made up of collagen (a protein found in connective tissue) that connect the various skull bones (Gray 1878, Tang *et al* 2008). They are wide to allow movement at birth, and remain open at various stages of development, differing between cases. For example, the frontal suture fuses between 3 and 9 months old (Vu *et al* 2001), whilst the sphenosquamosal suture usually closes by 6 years, but can take as long as 10 (Idriz *et al* 2015). In comparison, during adulthood, the coronal, sagittal, lambdoid, and squamosal sutures do not close until approximately 45, 50, 55, and 70 years of age, respectively (Singh *et al* 2004, Nakahara *et al* 2006, Idriz *et al* 2015, Kumar *et al* 2018, Russell and Russell 2018). An exemplar diagram of the adult skull sutures and their positions are displayed in figure 1. Neglecting the presence of sutures, which have differing conductivity to spongiform and compact bone (Tang *et al* 2008), can thus result in large and localised EEG source

reconstruction errors. Previous research has evaluated the impact that infant fontanelles have on EEG source analysis, which, although geometrically larger in comparison, is hypothesised to yield similar results when accounting for adult sutures. For example, Lew *et al* (2013) revealed that omitting the fontanelles but assuming correct skull conductivity (compared to a model with equivalent skull conductivity and fontanelle inclusion) produced maximum EEG source errors of 3.6 mm. A recent study further confirmed that the exclusion of fontanelles in neonates resulted in the largest source localisation errors directly below the fontanelles (Azizollahi *et al* 2020). Previously, Darbas *et al* (2019) similarly concluded that including the fontanelles significantly improved EEG source reconstruction. They also revealed conductivity variation near to the fontanelles and that eccentricity and orientation of dipolar sources significantly influenced EEG source localisation. The effect of adult sutures in EEG source analysis, however, has yet to be assessed.

Realistic head modelling, particularly of the skull, is therefore evidently an essential aspect of EEG forward and inverse computation. Numerical methods, as opposed to analytical approaches, are required to account for a realistic head shape, allowing for multiple non-spherical compartments. The finite element method (FEM) is one such numerical approach that can consider realistic models of arbitrary geometry, being able to incorporate anisotropy and heterogeneity between tissues, an advantage over other existing numerical approaches, such as the boundary element method (BEM; Vorwerk *et al* 2012). The BEM approximates the head as compartments with isotropic conductivities and computes EEG surface potentials produced by current sources at the interface and boundary of a homogeneous volume conductor. Importantly, FEM, differing from BEM, can additionally distinguish between spongiform and compact bone and accurately incorporate cerebrospinal fluid (CSF) without substantially increasing computation complexity, as well as represent a homogeneous skull, such as including the sutures (Vorwerk *et al* 2012, Beltrachini 2019). FEM is therefore frequently employed for EEG forward analysis utilising realistic and inhomogeneous conductivities and is integrated into known EEG analysis toolboxes such as FieldTrip (Oostenveld *et al* 2011) and BrainStorm (Tadel *et al* 2011).

This paper aims at evaluating the contribution that adult sutures have on the EEG forward and inverse solutions and their effect compared to neglecting deviations in bone composition. A detailed head model with inhomogeneous conductivity profiles that accounted for spongiform bone distribution throughout the skull and the presence of four adult sutures was developed. The FEM was then utilised to simulate the FP solution. Source analysis employing the 'true' inhomogeneous skull conductivity



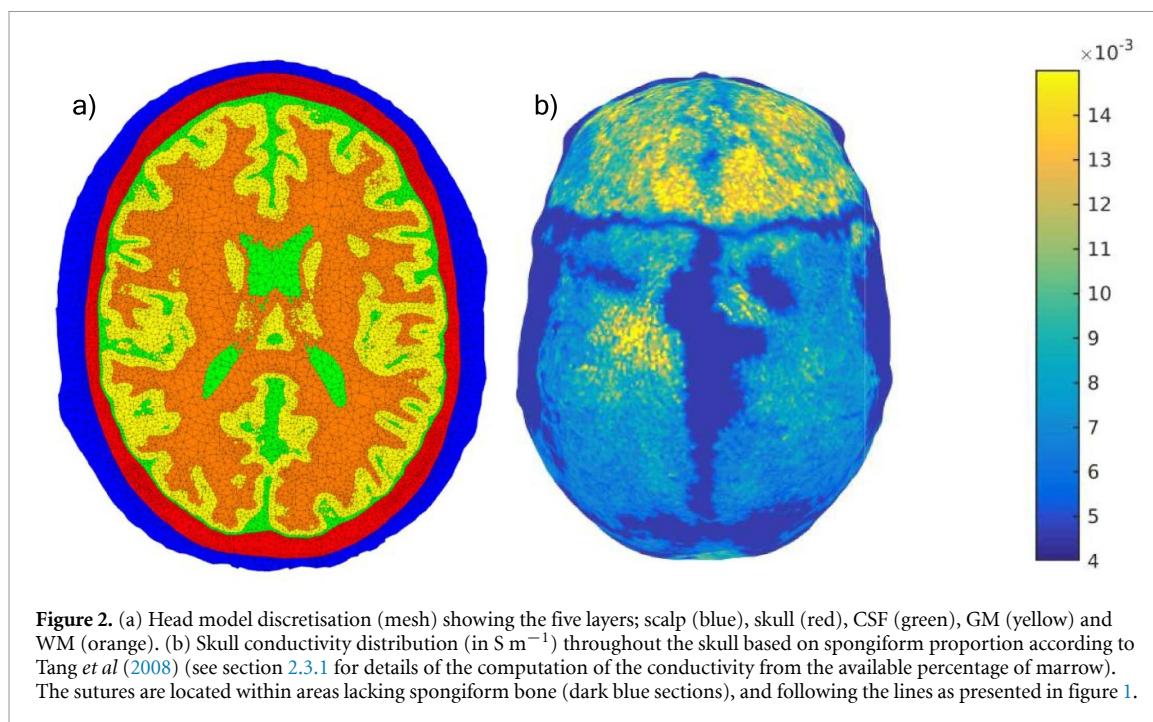
model was compared to simplified representations omitting the sutures and bone composition distribution. Homogeneous model conductivity values frequently employed in the literature were also used for comparisons. Moreover, aging skull conductivity profiles that accounted for variation in conductivity and suture closure with age were simulated to determine source analysis differences considering participant age. The results therefore highlight the importance that geometrically accurate head models with appropriate electrical conductivity are for EEG source localisation, with particular focus on the critical inclusion of adult sutures.

The paper is organised as follows. The generation of the utilised head model, including tissue segmentation, calculation of bone composition proportion and suture position assignment, is described in section 2.1. An outline of each of the experiments, including the model comparisons and their justifications is provided in section 2.2. The computation methodology for the models employed in each of the experiments (as described in section 2.2) is discussed in section 2.3. Specifically, section 2.3.1 details the generation of the ground truth model, section 2.3.2 outlines an electrical impedance tomography (EIT) protocol for estimating homogeneous conductor models and section 2.3.3 describes development of the age-appropriate skull conductivity models. Section 2.4 described the forward and inverse solution methodology and error measurements. The results are provided in section 3, discussing the contribution of the sutures and bone composition in section 3.1, the impact of different homogeneous models in section 3.2 and the results of the age-appropriate models in section 3.3. Finally, a discussion of these three main results is provided in sections 4.1–4.3, respectively, with considerations for future research in section 4.4.

2. Methods

2.1. Head model construction

A realistic detailed head model was developed from the high-resolution Colin27 MRI segmentation (Aubert-Broche *et al* 2006). Colin27 provided the segmented head model, which utilised combined T1 and T2 MRI data from repeated scans of a single participant with CT and MR angiography to provide better bone and vascular structure segmentation as well as high resolution (Aubert-Broche *et al* 2006). FreeSurfer (Fischl 2012) was then employed to compute the surface where the sources were placed, residing in the grey matter (GM), by calculating the midpoint between the GM/WM and GM/CSF interface (as described in section 2.4). This, together with the segmentations provided by the Colin27 atlas, resulted in five compartments: scalp, skull, CSF, GM, and WM. Further refinement provided bone marrow classification, enabling the creation of a detailed inhomogeneous skull map. The ISO2Mesh toolbox (Fang and Boas 2009) was then utilised to first compute surface meshes from the available segmentations. These meshes were subsequently employed to build a 3D tetrahedral discretisation resulting in 6.8 M elements and 1.1 M nodes into the five compartments (figure 2(a)). Each compartment and the resultant head model were manually checked for abnormalities and to ensure high quality of the mesh. Special refinements of the skull layer (0.4 M nodes) allowed for inclusion of differing bone composition and adult sutures by changing the individual element's conductivity. To calculate the percentage of spongiform and compact bone, the points at all interfaces between skull/CSF and skull/scalp were firstly computed. For each point on the skull/CSF interface, a straight line perpendicular to the interface was drawn until reaching the skull/scalp interface. The



percentage of spongiform bone at that point was then determined as the percentage of the line belonging to the soft bone compartment (based on the segmentation). Figure 2(b) displays the skull conductivity distribution as a function of spongiform bone proportion, computed according to Tang *et al* (2008) and further described in section 2.2.1. The presence of sutures was evidenced by the lack of spongiform bone in the corresponding regions and were clearly visible in the model, which merged CT and MRI data. The suture segmentation also followed the standard locations as displayed in figure 1. On the surface of the scalp layer, a total of 164 (point) electrodes were positioned according to the ABC-160 positioning system (BioSemi B.V., Amsterdam, Netherlands), plus an additional four fiducials (nasion, inion, left and right pre-auricular).

The adult sutures were manually segmented and incorporated into the head model. Skull elements along the suture lines and without spongiform bone (and thus assumed most likely to be sutures) were extracted and visualised using Matlab (Natick, USA). This visualisation confirmed the suture location was according to previously defined anatomical landmarks (Miura *et al* 2009; see also figure 1). The intersecting points where the generated sutures meet (i.e. bregma, lambda, asterions, and pterions) were then found. Elements along the path connecting the intersections with the least proportion of spongiform bone, and following previously defined anatomical landmarks, were manually selected and interpolated. All the elements fully composed of hard bone and with centroids at 10 mm from the sutures were considered part of them. This was done to comply with the conductivities provided by Tang *et al* (2008), which were measured in samples of approximately

that size. This produced five subject-specific anatomically correct non-smooth sutures: the sagittal, coronal, lambdoid, and the left and right squamous (see figure 1). These were defined as either dentate (sagittal, corona, and lambdoid) or squamosal (squamous), which have differing properties and thus conductivities (Gray 1878, Tang *et al* 2008).

The electrical conductivities of the scalp, CSF, GM and WM were assigned as 0.4137, 1.7358, 0.3787 and 0.1462 S m^{-1} , based on McCann *et al* (2019). The conductivity assignment of the skull for each model, including that of the sutures, is described in section 2.2.

2.2. Experiments

The electrical conductivity of the skull was varied to develop differing volume conductor models and demonstrate the impact such simulated deviations have on the EEG forward and inverse solutions. A ground truth model was first generated, which incorporated variation in spongiform and compact bone distribution throughout the skull, as well as the presence of sutures. The corresponding models were variations of the ground truth model, deviating according to skull conductivity alone. All models are summarised in table 1. The experiments comparing the various models and their purpose are outlined below. The methodology involved for generating each of these models is outlined in section 2.3 and the forward and inverse solution computation and comparison calculations between models is described in section 2.4.

2.2.1. Omitting sutures

The ground truth model (generation outlined in section 2.3.1) was compared against a model in which

Table 1. A summary of each employed model, outlining the distribution (homogeneous or heterogeneous), the computation of the whole skull conductivity, not including the sutures (either homogeneous with one conductivity or accounted for spongiform proportion variation), the conductivity of the sutures and how they were computed, and the model utilised for comparison in the FP and IP computation and the purpose and research aims of each model. All conductivity values are in $S\ m^{-1}$ if not explicitly mentioned.

Model	Distribution	Whole skull	Sutures	F/IP comparison model	Aims to highlight
Ground Truth	Heterogeneous	Computed according to spongiform proportion	Dentate—0.0173 Squamous—0.0079 Equal to hard bone	NA	Reference model
Omitting Sutures Neglecting Spongiform	Heterogeneous Homogeneous	Whole skull	0.0061 $S\ m^{-1}$	Ground Truth Omitting Sutures	Importance of including sutures Discrepancies when spongiform omitted
Homogeneous 0.01 $S\ m^{-1}$	Homogeneous	Whole skull	0.01 $S\ m^{-1}$	Ground Truth	Errors when assuming high homogeneous value
Homogeneous 0.0055 $S\ m^{-1}$	Homogeneous	Whole skull	0.0055 $S\ m^{-1}$	Ground Truth	Errors when assuming a low conductivity value
Homogeneous EIT Estimated	Homogeneous	Whole skull	0.0072 $S\ m^{-1}$	Ground Truth	Errors when providing ‘optimum’ homogeneous value
20 Years Old	Heterogeneous	Scaled function of ground truth to account for age variation	Scaled according to figure 3 to account for state of closure at different ages	Scaled homogeneous value estimated from EIT as described in section 2.3.2	Effect of omitting the sutures for each age when considering approximate conductivity of aging skull
30 Years Old	Heterogeneous				
40 Years Old	Heterogeneous				
50 Years Old	Heterogeneous				
60 Years Old	Heterogeneous				

the distribution of spongiform and compact bone was that of the ground truth, but the presence of sutures was neglected, and their conductivity considered that of hard bone. This experiment set out to determine the impact solely omitting the sutures, whilst accounting for variation in overall bone composition has on EEG source analysis.

2.2.2. Neglecting spongiform

The model omitting the sutures (but with spongiform distribution intact) was compared against a homogeneous skull conductivity model that did not account for bone composition variation nor the presence of sutures. The homogeneous skull conductivity was calculated as a global representation of the model that omitted the sutures utilising EIT (method described in section 2.3.2). This produced a one-layered skull conductivity value not influenced by sutures, and assuming no bone composition variation throughout the skull. The appraisal between this homogeneous model and that omitting the sutures aimed to assess the impact neglecting spongiform distribution variation throughout the skull had on EEG-FP and IP solutions. Comparing against the model omitting the sutures ensured any discrepancies were solely due to disregarding the variation in spongiform proportion, rather than also accounting for adult sutures.

2.2.3. Homogeneous 0.01 and 0.0055 S m⁻¹

The ground truth model was assessed against two models where the skull was assumed as one homogeneous layer with a single conductivity, taken from existing literature: either 0.01 S m⁻¹ or 0.0055 S m⁻¹. These comparisons aimed to indicate potential global inaccuracies when not accounting for inhomogeneity and taking a literature value as the truth, a very common practice in the field. The first homogeneous value (0.01 S m⁻¹) was extracted as the most frequently employed value in existing literature (Dannhauer *et al* 2011) and highlighted EEG source analysis discrepancies for a relatively high assumption of skull conductivity. The second homogeneous literature value (0.0055 S m⁻¹; Fernández-Corazza *et al* 2017) aimed to reveal such errors when assuming low skull conductivity, potentially in contrast to the previous high homogeneous value.

2.2.4. Homogeneous EIT estimated

The ground truth model was evaluated against a homogeneous skull model, where the global conductivity was estimated using an EIT protocol that accounted for variation in spongiform proportion and the presence of sutures (protocol described in section 2.3.2). The EIT homogeneous model aimed to provide a 'best guess' of a homogeneous volume given the ground truth model input, rather than assuming specific values according to previous literature. This experiment set out to determine EEG-FP and

IP solution inaccuracies when analysing discrepancies between homogeneous and inhomogeneous (i.e. the true) skull models.

2.2.5. Age estimated models

A separate set of experiments was carried out to determine the impact that not accounting for suture closure according to age has on EEG source analysis. The same realistic head model geometry (as described in section 2.1) was utilised, and five age-appropriate volume conductor models created from this identical geometry at 20, 30, 40, 50, and 60 years of age. For these models, only the conductivity of the skull differed from the ground truth model as we hypothesised a general decline in global skull conductivity and suture closure with age (computation outlined in section 2.3.3). An identical head geometry was thus employed for all age-appropriate models (please see section 4.3 for a discussion on the necessity of additional data and research for more accurate age-appropriate representations). Source analysis for each of the hypothesised age models were compared to those of an EIT estimated homogeneous skull conductivity value for each corresponding age (where the input for EIT estimation was the hypothesised age-appropriate model, as described in the EIT protocol in section 2.3.2). These evaluations aimed to elucidate the effect sutures has on EEG source localisation when an aging skull is taken into account.

2.3. Model computation methodology

This section describes the methodology employed to generate each of the volume conductor models. The computation of the ground truth model is outlined in section 2.3.1. The EIT protocol utilised to estimate the model neglecting spongiform, the homogeneous EIT estimated model and the age-appropriate homogeneous models that were used as comparison models for the hypothesised inhomogeneous age estimated models is described in section 2.3.2. The development of the heterogeneous age estimated models is outlined in section 2.3.3.

2.3.1. Ground truth model

The ground truth model was regarded as the reference and absolute truth, where the proportion of spongiform and compact bone throughout the skull and the sutures were accounted for. The skull conductivities were taken from Tang *et al* (2008), where resistivity measurements were extracted from 388 excised skull samples of differing structure. These values were utilised as they represented the most comprehensive average conductivity values from a large sample size, across varying participants and skull regions using a robust method. The employed methodology was assessed in a recent meta-analysis (McCann *et al* 2019) and regarded as high quality in a Quality Assessment due to measurements being obtained from freshly excised tissue, in a carefully controlled

situation, at stable (body) temperature and across many participants.

The sagittal, coronal, and lambdoid sutures were assigned the average conductivity for dentate sutures, i.e. 0.0173 S m^{-1} . The squamous sutures' conductivities were assigned the average reported values, i.e. 0.0079 S m^{-1} . The conductivity of the remaining skull was modelled as a function of the cross-sectional proportion of spongiform bone. This was taken from figure 6(b) of Tang *et al* (2008), where $\sigma^{-1} = 215 - 231.25 \times p$, with p being the spongiform thickness percentage. This corresponds with the effective-medium approximation for the effective conductivity of a material given a number of compartments with different conductivities (Torquato and Hyan 2001). The maximum value of p was set to 80% to account for the fact a skull region cannot be completely spongiform. Compact bone was modelled with a conductivity value of $0.003787 \text{ S m}^{-1}$. This resulted in an inhomogeneous skull conductivity model incorporating sutures and deviations in skull composition, termed the ground truth model.

2.3.2. EIT protocol

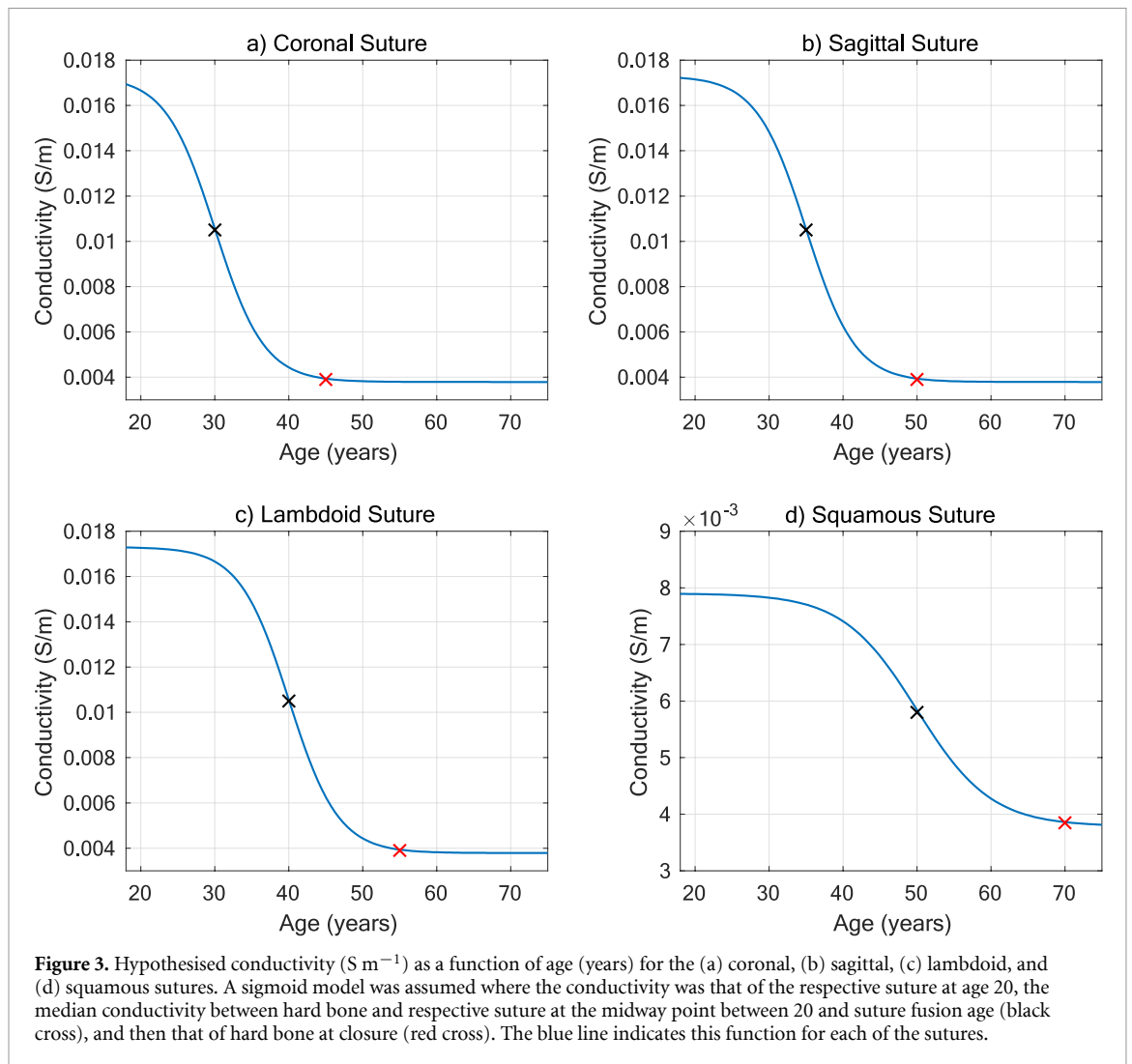
Models employing a personalised homogeneous skull layer were estimated using an EIT simulation protocol (Fernández-Corazza *et al* 2017). EIT is a non-invasive imaging modality where electrical conductivity is estimated following current injection between electrodes and measurement of the resultant electric potentials from the remaining electrodes. The EIT current injected can be simulated given an input volume conductor model and the global conductivity of each compartment (e.g. the skull) estimated. EIT was thus utilised to approximate homogeneous skull conductivity values, given an inhomogeneous input model. The employed Colin27 input model was either the ground truth, the model omitting sutures, or one of the five hypothesised age-appropriate models. For all the input models, the conductivities of the scalp, GM, white matter (WM), and CSF were fixed according to the literature (see section 2.1) and only the skull conductivity was estimated. This was as the current study aimed to focus on the contribution of variation in skull conductivity alone.

For each of the EIT estimation protocols, first the ideal EIT measurements were computed based on the reference input model. This was thus the most detailed model and was either the ground truth, the model omitting sutures or one of the five age-appropriate models (as above). The conductivity value for the skull as one homogeneous (and thus simplified) compartment was then determined using EIT simulation. The current injection was simulated between electrodes located on the scalp of the appropriate model and the conductivity estimated from simultaneous potential recordings. A current amplitude of 0.25 mA was passed from one 'source' to one 'sink' for 32 pairs of electrodes, located on the scalp of

the model, optimised so that the injection points were at the most maximum distance from one another (Mamatjan *et al* 2012). These pairs were evenly distributed across the skull and utilised a pair number (32) in typical EIT systems (McCann *et al* 2011, Oh *et al* 2011, Khan *et al* 2014, Avery *et al* 2017). The resulting voltage was calculated on the remaining electrodes not involved in current injection (called EIT-FP) and used to estimate the equivalent conductivity (referred to as EIT-IP). The EIT-FP was solved numerically using the FEM and a preconditioned conjugated gradient (PCG) algorithm, with LU (lower-upper) factorisation matrices (factoring a matrix as the product of an upper and lower triangular matrix) as preconditioners, as described in Fernández-Corazza *et al* (2013). The EIT-IP then estimated the compartmental electrical conductivity from the simulated potential measurements using the least squares approach to minimise the ℓ_2 -norm of the difference between measurements and model estimations. The quasi-Newton numerical optimisation method was utilised to solve this due to less iterations required and higher stability. It has been previously shown that employing initial values lower than the true conductivity further increases stability and convergence speed to the global minimum (Fernández-Corazza *et al* 2017). Thus, the initial guess for skull values was set to 0.005 S m^{-1} . The final homogeneous value was taken as an average of estimations from all injection pairs, providing a global and homogeneous estimate (as carried out in Fernández-Corazza *et al* 2017). A more detailed description of an EIT protocol is described in Fernández-Corazza *et al* (2013, 2017).

2.3.3. Age-appropriate models

Five age-appropriate models at 20, 30, 40, 50 and 60 years, were created to account for general decline in global skull conductivity (Antonakakis *et al* 2020, McCann and Beltrachini 2021) and suture closure with age. The estimated decrease with age was taken from the mean function in McCann and Beltrachini (2021; figure 1(a) in that publication). The relationship was computed according to the data acquired in Gonçalves *et al* (2003a, 2003b) and chosen in the current study as they utilised an EIT method, similar to our homogeneous EIT estimations. Bone composition and the resulting conductivity distribution were firstly modelled as in the ground truth model. The whole conductivity distribution, accounting for variation in spongiform and compact bone proportion, was then scaled for each age according to the sigmoid function described in McCann and Beltrachini (2021; figure 1(a)). The sigmoid function from McCann and Beltrachini (2021; figure 1(a)), further justified in that publication, was first assumed as the general function describing decline in whole skull conductivity. This distribution was then adjusted and scaled accordingly, so the global conductivity value estimated from



the function, at age 28 (the age of Colin27 at scanning; Aubert-Broche *et al* 2006), aligned with the EIT estimated homogeneous value of the Colin27 model. This standardised the hypothesised aging skull conductivity with the estimated homogeneous conductivity of the utilised volume conductor model (Colin27). As a result, a final function describing the decline in conductivity with participant age was thus determined, where $T_{sc} = T \times 0.0187e^{\text{age} \times -0.0268}$. Here, T is the vector describing the conductivity distribution in the skulls' tetrahedra according to bone composition (as computed from Colin27 and described in section 2.1) and T_{sc} is the new distribution according to modelled age. The scale is thus determined by participant age at $0.0187e^{\text{age} \times -0.0268}$.

The closure of the adult sutures was then modelled considering fusion at 45, 50, 55, and 70 years for the coronal, sagittal, lambdoid and squamosal sutures, respectively, as mentioned in the literature (Singh *et al* 2004, Nakahara *et al* 2006, Idriz *et al* 2015, Kumar *et al* 2018, Russell and Russell 2018). The sutures were assumed to close at a sigmoid rate from age 20, in accordance with previous publications (figures 3–5 in Todd and Lyon 1925; figure 3 from

Jangietriew *et al* 2007; and figure 3(a) from Chiba *et al* 2013). This choice was additionally supported by Ruengdit *et al* (2020), who reviewed cranial sutures' closure. They found that the sutures typically progress slowly in early adulthood from age 20, then rapidly until approximately $\frac{3}{4}$ of the age at complete closure, and finally slowly again towards absolute fusion age. The conductivities at age 20 for all suture types were assigned according to Tang *et al* (2008), whereas the values at closure were assumed as that of hard bone.

The resultant conductivities of the sutures as a function of age are depicted in figure 3. From age 20 to closure age, a sigmoid function was generated where conductivity equalled the median between that of hard bone and the respective suture at the midway point between age 20 and suture fusion.

2.4. EEG forward and inverse problems

The EEG-FP was solved using the FEM and the analytical subtraction approach (Beltrachini 2019) with a PCG algorithm and LU factorisation matrices as preconditioners. This method has been previously shown to perform well compared to other subtraction-based approaches and was the most

robust against deformation of individual elements and eccentric sources (Beltrachini 2019). A detailed explanation of this solver can also be found in Beltrachini (2019). A total of 20 119 sources were placed centrally in the GM compartment. This was done by computing the mid surface between those corresponding to the GM/CFS and GM/WM interfaces provided by FreeSurfer (Fischl 2012). All source positions were checked to belong to the resulting GM compartment. Normal restraint is a reasonable physiological assumption due to the fact apical dendrites produce a measured field oriented normal to the surface (Baillet *et al* 2001). Furthermore, when the head model is known from MRI/CT data and is considered as a true, not approximate, model with pre-defined source positions, normal constraint is realistic and frequently employed (Grech *et al* 2008, Valdés-Hernández *et al* 2009). Average reference was considered in all simulations.

The standardised low resolution electromagnetic tomography (sLORETA) method was used to solve the EEG-IP (Pascual-Marqui 2002) given the electrical potential input as estimated from the EEG-FP (see above). This employs the current density estimate provided by a standardisation of the minimum norm solution to infer localisation based on these estimates. sLORETA calculates the smoothly distributed electric activity whilst assuming synchronous and simultaneous neuronal firing of adjacent neurons and no noise and is thus capable of exact (zero-error) localisation under specific scenarios (Pascual-Marqui 2002). The method computes the equivalent dipole location as the maximum measurements of the standardised power. sLORETA was chosen due to its discussed capability of yielding zero localisation error when utilising the actual head model and assuming no noise, as well as a reduced likelihood of locating deep sources as residing on the surface (as with minimum norm estimation). Furthermore, non-standardised LORETA can result in zero electrical activity estimation at superficial sources, which sLORETA avoids (Pascual-Marqui 2002).

The EEG-FP was solved for all proposed models. Comparisons were made between the FP electric potentials of two models, as necessary for the experiments outlined in section 2.2. The relative error (RE) metric was employed to characterise errors in the FP, defined as $RE = \|u_t - u_n\| / \|u_t\|$, where u_t and u_n are the potentials generated by a given source employing the input and approximated models, respectively. The RE describes the overall difference between the two employed models. The magnification factor (MAG) was also computed to indicate the errors in magnitude between the two comparison models, where $MAG = \|u_t\| / \|u_n\|$. The relative difference measure (RDM) was additionally calculated as a measure of topographical error with minimal error as $RDM = 0$. Here, $RDM = \|(u_t / \|u_t\|) - (u_n / \|u_n\|)\|$. The MAG and RDM results are displayed

in the supplementary material (available online at stacks.iop.org/JNE/19/016014/mmedia). These error measurements are frequently used in addition to RE within EEG analysis fields (Wolters *et al* 2006).

The EEG-IP was solved for each generated lead-field given the potentials calculated for the input model. For each source, the distance between estimated locations using the input and approximated models was calculated, to result in an absolute error (AE, measured in cm) between the input and comparison models (according to the required models for each experiment, described in section 2.2).

3. Results

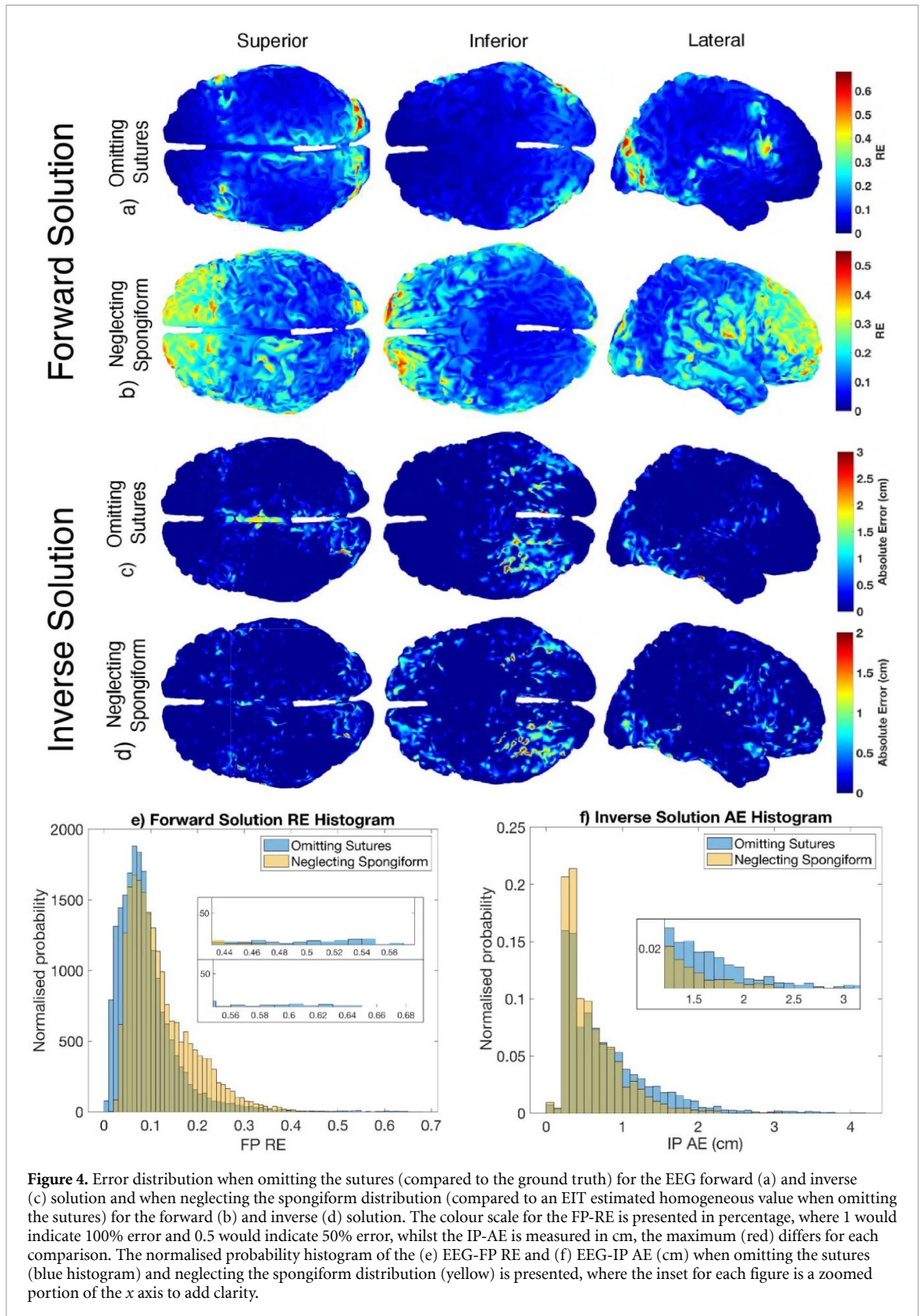
The EIT estimated homogeneous skull conductivity for the model neglecting spongiform proportion was found to be 0.0061 S m^{-1} . When accounting for a 'ground truth' of both variation in bone composition and the presence of sutures the EIT estimated homogeneous model conductivity was estimated as 0.0072 S m^{-1} . Hypothesised age-appropriate homogeneous skull conductivity values considering both spongiform proportion and sutures were estimated as $0.0086, 0.0068, 0.005, 0.0037, 0.0029 \text{ S m}^{-1}$ for 20, 30, 40, 50 and 60 years old, respectively.

3.1. Impact of sutures and bone composition

As can be seen in figure 4, omitting the presence of sutures, compared to the ground truth model, resulted in the largest FP-RE (figure 4(a), maximum 67.72%) and IP-AE (figure 4(c), maximum 4.14 cm) across the suture lines, particularly the dentate. Figure S1 in the supplementary material equally displays high MAG and RDM values across suture lines, particularly noticeable across the dentate sutures. When neglecting variation in spongiform and compact bone distribution throughout the skull, the greatest FP-RE (maximum 47.47%) and IP-AE (maximum 2.19 cm) was evident across areas of high spongiform proportion, particularly in frontal regions (figures 4(b) and (d), respectively). Deep sources also produced relatively large IP-AEs (figure 4(c), inferior view). Highest MAG values were revealed in high spongiform proportion areas (figure S1(b)), with low values in high compact bone (figure S1, lateral view). Topological errors were decreased compared to magnification factor values when neglecting the spongiform proportion (figure S1(d)). Omitting the sutures produced the largest maximum and localised forward solution errors for both the FP (figure 4(e), inset) and IP (figure 4(f)). However, neglecting spongiform proportion resulted in higher global FP errors than omitting the sutures (figure 4(e)).

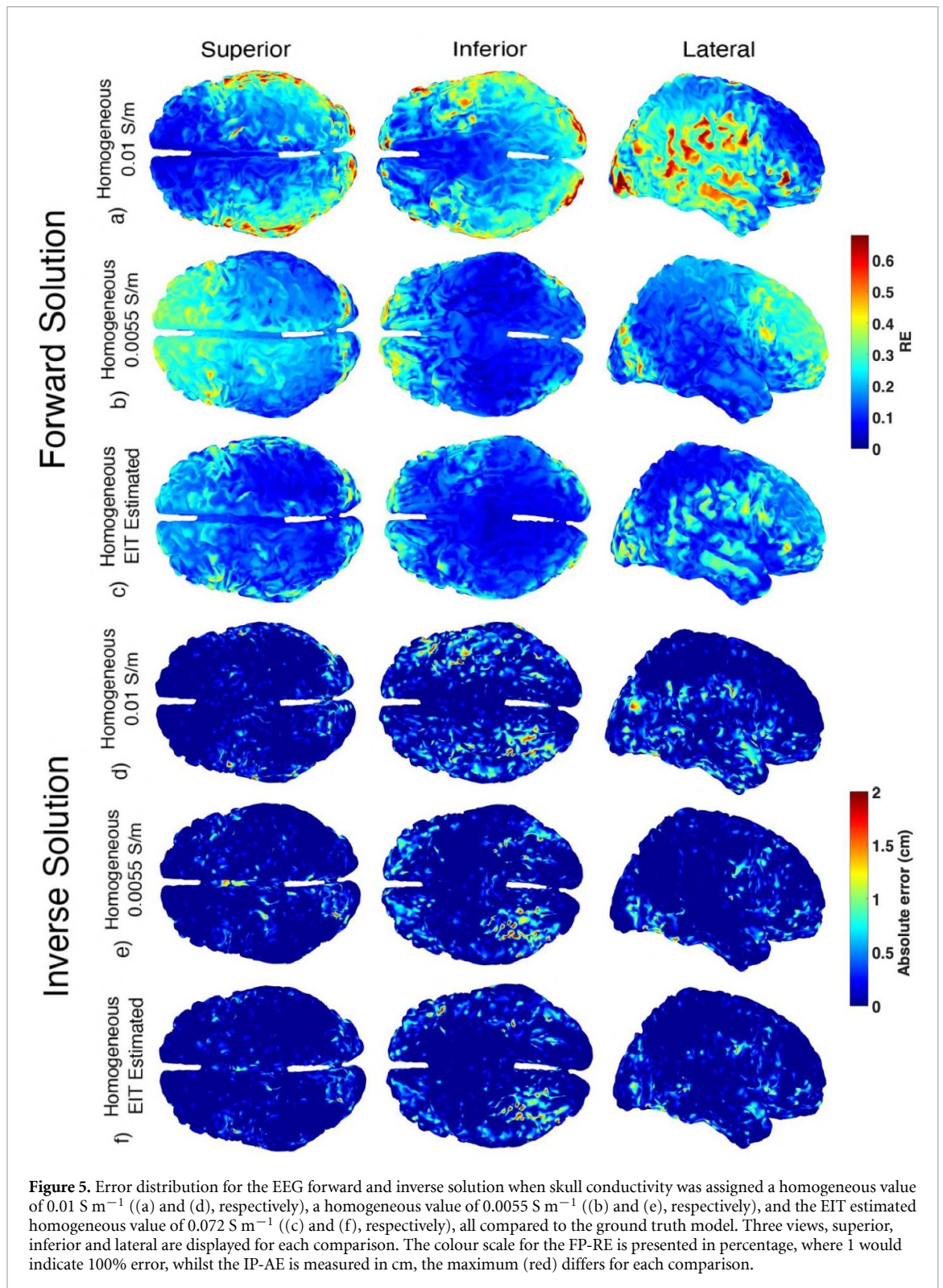
3.2. Homogeneous skull models

Figure 5 indicates that assigning the most frequently employed homogeneous skull conductivity value (0.01 S m^{-1}) produced the greatest FP (maximum



85.49%) and IP (maximum 2.7 cm) error across complete compact bone regions (figures 5(a) and (d) for the FP and IP, respectively). This also produced the largest maximum FP-RE of all the computations, most notably in the temporal and lower parietal regions. Comparably, assigning a lower value (0.0055 S m⁻¹) resulted in the largest FP (maximum

56.81%) and IP (maximum 3.03 cm) errors across areas of high spongiform proportion, particularly pronounced in the frontal cortex, and through suture lines (figures 5(b) and (e) for the FP and IP, respectively). Similar results were revealed for magnitude errors, with high MAG values across high areas of spongiform bone for the 0.0055 S m⁻¹ model



(figure S2(b)) and low values across high compact bone proportion for the 0.01 S m^{-1} model (figure S2(a)). The EIT estimated model produced relatively lower overall MAG in both high spongiform and compact bone, similar to RE (figure S1(c)). The greatest topographical error were across areas of particularly high spongiform or compact bone proportion (figures S2(d)–(f)). Of the three homogeneous skull models, the EIT estimated value produced

the lowest RE and AE, with the greatest FP (maximum 53.28%) and IP (maximum 3.03 cm) solution error across regions of very high (i.e. frontal areas) or no (particularly temporal regions) spongiform proportion (figures 5(c) and (f) for the FP and IP, respectively). The EIT estimated homogeneous model generated the lowest overall distribution of FP and IP error of the homogeneous models (figure 6).

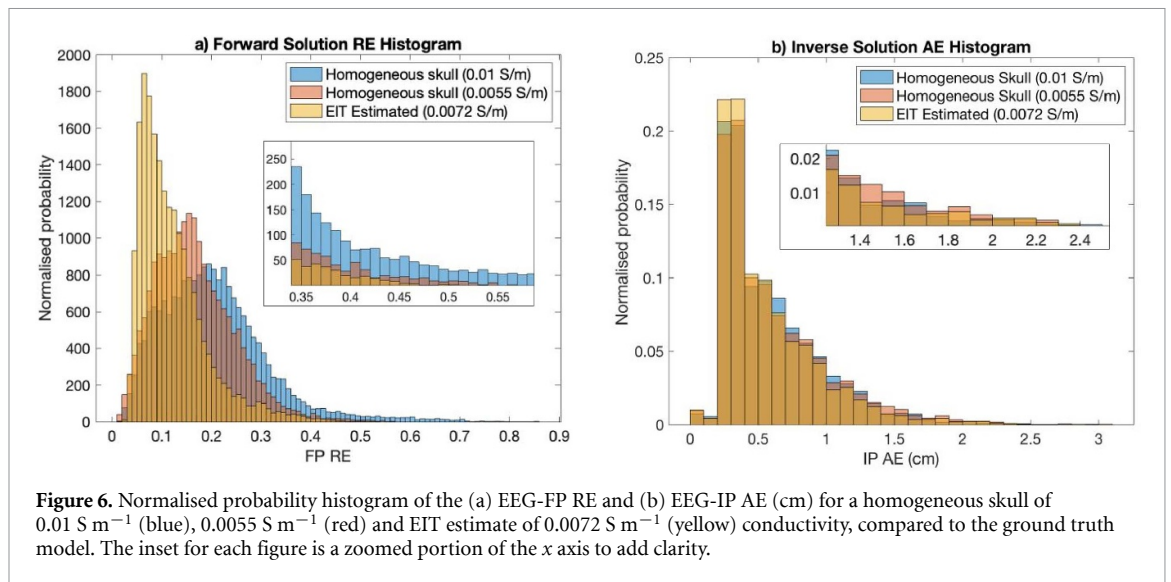


Figure 6. Normalised probability histogram of the (a) EEG-FP RE and (b) EEG-IP AE (cm) for a homogeneous skull of 0.01 S m^{-1} (blue), 0.0055 S m^{-1} (red) and EIT estimate of 0.0072 S m^{-1} (yellow) conductivity, compared to the ground truth model. The inset for each figure is a zoomed portion of the x axis to add clarity.

3.3. Age-appropriate models

The forward and inverse solution error between the hypothesised age-appropriate models (ages 20–60) and their respective EIT estimated age-appropriate homogeneous value are depicted in figure 7. The largest FP-RE for all (with the exception of the 30 year old models experiment, due to similarity with the corresponding EIT estimated model) was revealed across regions of high spongiform proportion, in the frontal brain area. The greatest FP-RE for the 30 year old model was across suture lines, as in the model omitting sutures (see figure 5(b)). Errors across suture lines were also evident for the 20 and 40 year old model experiments (figures 7(a) and (c)), particularly across the lambdoid and coronal sutures, whilst FP-RE can be seen along the squamous suture for the 50 year old (figure 7(d)). The MAG value was revealed to be low across high areas of spongiform bone (the frontal region) and greater across areas of high compact bone (temporal areas), as can be seen in figure S3 (MAG values) for all of the age-appropriate models. The topographical (RDM) error revealed increased values in deep frontal sources and across higher compact bone areas, this was evident for all models (figure S3, RDM values). The greatest IP-AE for all ages, however, were in regions with the highest proportion of spongiform bone (frontal and right central areas) and at the base of the brain (see inferior view). The maximum FP-REs for the 20, 30, 40, 50 and 60 year old evaluations were 66.2%, 42.14%, 72.06%, 78.63% and 78.77%, respectively, whilst the maximum IP-REs were 1.95, 2.29, 2.04, 2.76 and 2.21 cm, respectively.

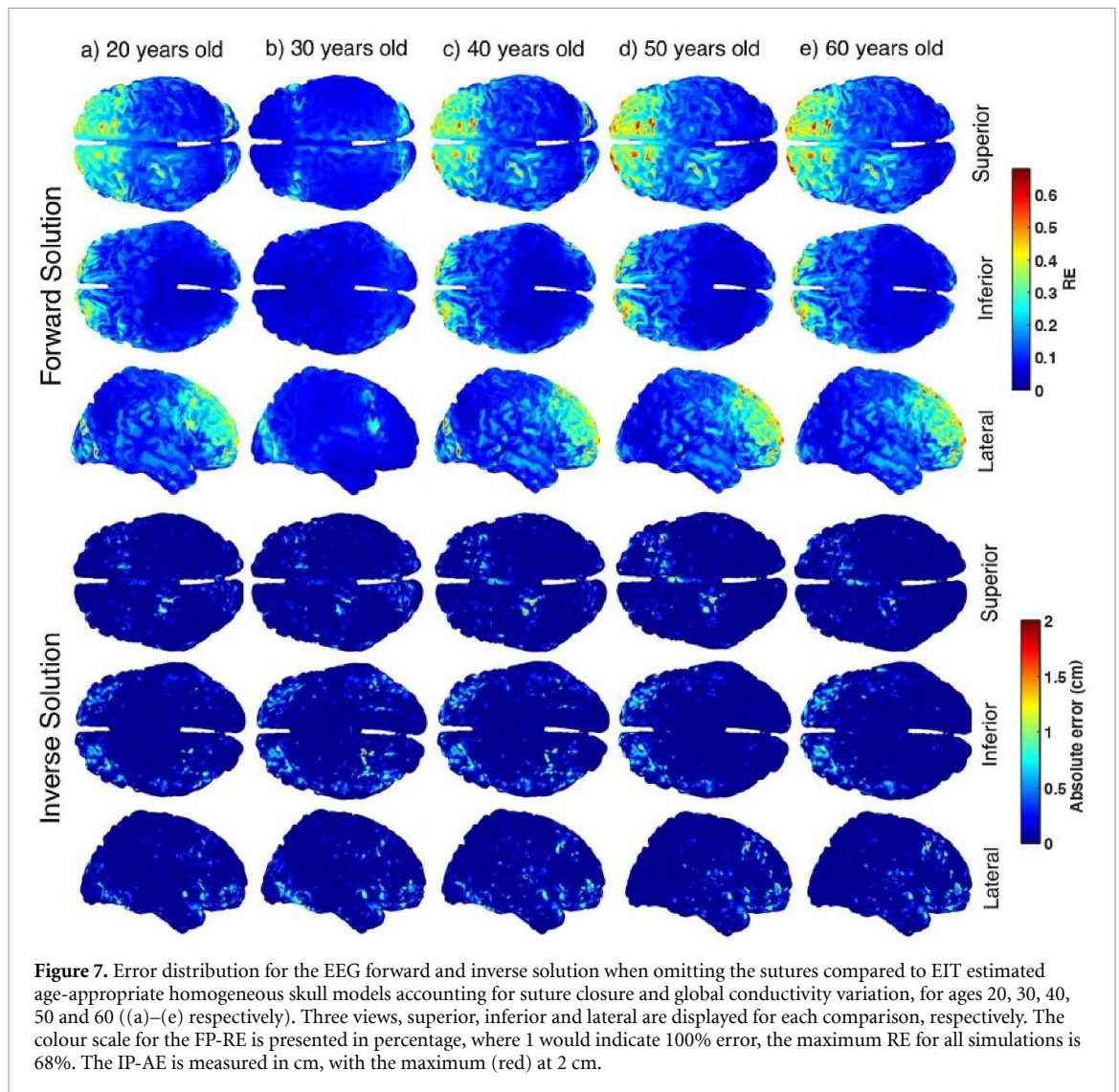
4. Discussion

The current study assessed the impact that neglecting adult sutures and differing bone composition has on EEG forward and inverse solutions. An inhomogeneous skull conductivity head model was

created that accounted for variations according to proportion of spongiform and compact bone as well as the presence of adult sutures. This model was compared to others omitting sutures and/or spongiform bone with differing homogeneous conductivity values. A hypothesised aging skull was further computed to assess the contribution of suture closure with age on EEG source computations. Our results revealed large forward solution relative errors, up to 85%, between models, particularly evident across suture lines when omitted and directly related to proportion of spongiform. Inaccuracies of up to 4.14 cm were revealed for the EEG inverse solutions when the sutures were not taken into account. Source localisation errors were also particularly related to proportion of spongiform and across suture lines. This result was not eradicated when an aging skull was estimated as significant FP errors across suture lines remained evident at ages 20–50 years old.

4.1. Impact of sutures and bone composition

The current results importantly elucidated the novel significance of adult sutures. When omitting the presence of sutures and considering them as compact bone, the highest forward and inverse inaccuracies were revealed directly beneath suture lines (see figures 4(a), (c) and S1(a), (c)). Specifically, when sutures were neglected, forward solutions may have a relative error of up to 67%, with erroneous source localisation of up to 4.14 cm. This is more evident for the dentate (coronal, sagittal and lambdoid) than squamosal sutures, where the conductivity of hard bone deviated further from the respective suture. Of note, omitting the presence of sutures resulted in the greatest general IP solution errors of the first five core experiments. Moreover, when accounting for variation in suture closure, as well as the deviation in whole skull conductivity according to age, the impact of sutures remained. Specifically, the dentate sutures resulted in noticeable FP-RE for



ages 20–40 years old (figures 7(a)–(c)), whilst the squamosal sutures retained a visible error for the hypothesised 50 year old (figure 7(d)). As when omitting the sutures (figures 4 and S1(a), (c)), this is due to the whole skull conductivity (as estimated with EIT) being closer to that of the dentate sutures for the 20–40 age ranges, whilst the opposite is true for the 50–60 range. Furthermore, results obtained with the hypothesised 30 year old head model are comparable to that of the model omitting the sutures, as the age of the utilised head model in all simulations is similar. Thus, significant differences between these models were not expected. These results suggest the influence of the adult sutures is not minimal and remains regardless of suture closure. In support of our results, Azizollahi *et al* (2016) varied fontanelle conductivity, which they suggested would decrease during infant development due to the ossification process. Skull conductivity decreases during the ossification process and causes the fontanelles to close and be replaced by less conductive bony structures (Lipsett *et al* 2019). Such variation in fontanelle conductivity

as in Azizollahi *et al* (2016), mimics the presented hypothesised deviation due to age in adult sutures and local REs beneath fontanelle lines were revealed. The forward solution errors were notably large particularly along suture lines which also corresponded to high magnitude errors, suggesting incorporating accurate suture conductivities is essential for determining electrical current propagation.

The exploration of sutures on EEG forward and inverse solutions has not yet been previously investigated, due to the necessity of CT data for accurate skull segmentation. Although the utilised head model represents one head alone and results may not be generalisable to the entire population, high resolution MRI and CT information has been employed providing essential contributions. This allowed representation of ten tissue types including four sutures, thus is considerably detailed compared to typical realistic models and permitted novel conclusions, such as the contribution of the sutures, to be made.

The presented results can be related to previous research discussing the influence of neonatal sutures

and fontanelles, which provided analogous findings. For example, Lew *et al* (2013) demonstrated the conductivity difference between the skull and fontanelles significantly impacted EEG forward and inverse solutions. They demonstrated source reconstruction errors were considerably lower than our study (maximum 2.4 mm). One explanation for this, as the authors mentioned, is the relative size of infant heads. Our study employed adult head sizes and inaccuracies from Lew *et al* (2013) may therefore be equivalent in adult heads and result in higher significance of the misspecification. There also exists additional differences between infant and adult head models such as the presence of large fontanelles, skull and scalp thickness, percentage of spongiform bone, CSF volume and GM/WM distribution which may account for such discrepancies. The current study employed a particular head model that did not account for complete differences between infant and adult head geometries, which is acknowledged as a limitation. Future research should implore to utilise accurate neonatal and infant head models for the most precise comparisons. Moreover, the conductivity values of all the compartment tissues differed considerably in Lew *et al*'s paper (2013), compared to our study. Of particular note is that of skull conductivity which was assigned a value of 0.04 S m^{-1} (or between a range of $0.03\text{--}0.05 \text{ S m}^{-1}$ for comparison models). This was more than double and, in some cases, quadruple any skull conductivity value utilised in the presented study. Additionally, Lew *et al* (2013) employed 277 EEG and MEG electrodes, compared to 164 in the current study, which may further contribute to localisation error differences. Such source localisation differences may also be explained by their use of unconstrained sources compared to normally constrained sources. In our study, normal constraint may have, in comparison, resulted in the higher source localisation areas. Additionally, a different IP methodology was employed, using a single dipole fit compared to sLORETA in our study, which may contribute to the inverse solution differences. Furthermore, in Lew *et al*'s (2013) study, the initial guess of the dipole fit was set to the original position and orientation, which may have also minimised the inverse solution errors.

Comparable local effects to our study, however, have additionally been revealed in previous research, where Azizollahi *et al* (2016) discovered forward errors directly below the fontanelles. Likewise, Lanfer *et al* (2012) found local defects in skull geometry, such as simulating sinuses as compact bone and skull holes resulted in forward and inverse miscalculations within the vicinity of the deficiency. This was additionally supported by Bénar and Gotman (2002), Vanrumste *et al* (2000) and more thoroughly in Von Ellenrieder *et al* (2014). High source localisation errors in the current study may, however, be also

somewhat explained by the use of normally constrained sources. As revealed in Valdés-Hernández *et al* (2009), normal constrained sources caused increased localisation errors when the head model was approximated due to potential large differences in the actual and approximate normal direction, as the normal may not point in the same direction. This is supported by a more recent study by Vorwerk *et al* (2019) where source reconstruction errors were reduced for sources with 'free' orientation and these errors, as a result of conductivity deviations, could be moderately compensated by source orientation modifications. The sources and head model in the current paper, however, were geometrically accurate and only the conductivity distribution of the head model was simplified. Thus, a lesser effect of normal constraint was assumed and was deemed suitable for the purposes of this study. Nevertheless, further research, particularly when the head model and participant MRI or CT is unavailable, or sources are unknown, as can be the case in infants, should consider utilising unconstrained moments to reduce such an impact of oriental differences.

It is noted that when neglecting the presence of sutures, the conductivity was assumed to equal that of hard bone, however, this may not be the case for all individuals. Furthermore, suture closure was assumed from literature data to decline in a sigmoid fashion. However, such closure may not relate directly to conductivity values. Knowledge of suture conductivity and their closure is limited from the existing literature, and therefore future research that explores this in more detail is imperative for detailed understanding and EEG source analysis. Alongside this, it is noted that skull conductivity values are taken from Tang *et al* (2008) alone or estimated from an EIT methodology (Fernández-Corazza *et al* 2017), which does not account for measurement variation across participants and studies and the relative quality of the utilised method. The true conductivity of the utilised head model (Colin27) will differ from these proposed values; however, this highlights the necessity of individualised conductivity measurements for the most accurate EEG forward and inverse computation. Furthermore, conductivities of soft tissues were assigned as the weighted average from McCann *et al* (2019), weighted according to the quality of each respective study. This provided the optimum conductivity value given the available data. Skull conductivity estimations were, however, not weighted as they were employed to highlight specific inhomogeneous differences. It is acknowledged that the quality and methodology (for example E/MEG compared to EIT protocols) will impact the obtained inhomogeneous skull conductivity values. Future studies may therefore utilise different techniques for obtaining conductivities and compare their effects on EEG forward and inverse computations.

The present simulations further revealed that neglecting an assumed variation in spongiform proportion resulted in maximum forward relative errors of 47% and maximum source localisation errors of 2.19 cm. As expected, this was considerably more evident across regions with high marrow bone concentration, particularly in the frontal skull regions as well as within the temporal lobe (figure 4(b)). Peak forward and inverse errors were greater when omitting the sutures than when neglecting spongiform variation. However, the relative forward error across the whole skull was more widespread (see figures 4(a), (b) and S1(b)). Overlooking differing bone composition indicates greater global error than omitting the sutures alone. This is supported by Lew *et al*'s (2013) results, where skull conductivity mismatch produced broader errors than excluding infant sutures and fontanelles. Comparable to our findings, previous research has revealed inaccurate skull segmentation of the compact and spongiform bone results in considerable forward and inverse solution errors up to 2 cm (Wolters *et al* 2006, Dannhauer *et al* 2011, Lanfer *et al* 2012, Montes-Restrepo *et al* 2014). Vorwerk *et al* (2014) notably revealed significant EEG source localisation errors within temporal regions, similar to our EEG-FP results (figure 4(b)), but not frontal areas. This may be explained by the specific distribution of spongiform bone, the proportion of which was high for our utilised model in both frontal and temporal regions. Neglecting the distinction between bone composition is thus hypothesised to result in increased FP and IP EEG errors in both high compact and spongiform regions, differing between participants and head models. Furthermore, the skull tissue conductivities utilised in Vorwerk *et al* (2014) were considerably higher and with a greater difference between compact and spongiform conductivities than in the presented study. For example, compact bone was assigned a value of 0.008 S m^{-1} (compared to our value of 0.0038), whilst areas of the highest spongiform bone proportion in our methodology reached a maximum conductivity of 0.014 S m^{-1} compared to 0.025 in Vorwerk *et al*. An approximately 2-fold difference between these values may explain differing results. This is alongside greater disparity between the spongiform, compact bone and whole skull conductivities in Vorwerk *et al* (2014) than the current study and thus larger errors would be present in high spongiform areas (such as the temporal lobe). Aside from this, our results are further supported by comparisons between homogeneous and inhomogeneous skull models, where using CT, heterogeneous skull conductivity yielded the lowest errors compared to homogeneous models (Sadleir and Argibay 2007, Dannhauer *et al* 2011, Montes-Restrepo *et al* 2014). Dannhauer and colleagues (2011) additionally showed that employing local heterogeneous models produced source localisation errors up to 4 mm, compared to 2 cm with global homogeneous models.

4.2. Impact of a homogeneous skull

As revealed in the study by Dannhauer *et al* (2011), as well as previous literature, assuming homogeneous skull conductivity values can result in significant propagated electric potential errors and source localisation (Vallaghé and Clerc 2008, Chen *et al* 2010, Acar *et al* 2013, Vorwerk *et al* 2019). Our results support these findings, where homogeneous skull models compared to the ground truth value lead to forward solution relative errors of up to 85% (for a homogeneous value of 0.01 S m^{-1}) and 57% (for a value of 0.0055 S m^{-1}). The region of greatest error also depended on spongiform and compact proportion distribution. For the 0.01 S m^{-1} homogeneous skull model, the highest errors occurred in areas of complete compact bone (with a conductivity of 0.0047 S m^{-1}). This is as expected as the homogeneous conductivity deviated further from compact than spongiform bone (with approximate conductivity between 0.013 and 0.016 S m^{-1}). Conversely, employing a lower homogeneous skull conductivity (0.0055 S m^{-1}) resulted in lower REs, with the highest miscalculation across regions of high spongiform proportion. This homogeneous conductivity deviated further from that of marrow than compact bone, hence the greatest errors were revealed across these areas. The presented results suggest forward solution errors may be a direct result of skull bone composition errors and the approximated homogeneous value. The highest proportion of marrow bone is across the frontal skull region (see figure 2), whereas the areas of complete compact bone are typically across temporal regions. Homogeneous conductivities considerably different from complete compact and high marrow bone values would yield the greatest forward solution errors within the respective regions. Notably, a higher homogeneous conductivity value in our study produced the greatest FP-REs of the first five core experiments. Our results suggest that, when assuming a homogeneous skull value, the differences between compact and marrow bone should be minimised.

EIT provided a method to estimate homogeneous skull conductivity and thus minimise eccentricities due to sutures and bone composition across a heterogeneous model. It computed the most likely homogeneous global conductivity value given an inhomogeneous model. The forward solution RE was smaller when utilising EIT estimated conductivity (0.0072 S m^{-1}), with a maximum error of 53% (figures 5(c) and 6(a)). Similarly, localisation errors were largely reduced for this model (figure 5(f)), producing the lowest IP-AE of the first five core experiments (figure 6(b)), with additionally lower MAG and RDM errors (see figure S2). However, this model did result in a maximum AE of 3.03 cm, marginally higher than a high homogeneous value and identical to the low value, assumed from the literature. As expected, regions with the greatest error were both in areas

of complete compact bone and the highest spongiform proportion. EIT estimated homogeneous conductivity, however, minimised deviations between the bone composition and thus produce less concentrated inaccuracies. This was particularly evident when compared with the high and low skull conductivity values, assigned from literature. EIT is typically considered non-invasive, safe, cost and time-effective, easily portable and acquired (Holder 1992) with relatively good skull conductivity characterisation, therefore it is suggested as one such method for easily obtaining individualised conductivity measurements. The presented EIT method may therefore be one technique to reduce errors incurred when assuming a homogeneous skull. The global homogeneous conductivity can be estimated during EEG acquisition, based on real EEG electrical potentials and solved accordingly (Gonçalves *et al* 2000), using a standard EIT application. Applying EIT during EEG acquisition to determine equivalent head tissue conductivities reduced systematic EEG-IP inaccuracies by up to 1 cm and obtained conductivities within 5% of the true value (Gonçalves *et al* 2000). This may be especially useful when MRI alone, and not CT or x-ray information, is available, essential to most accurately segment bone compartments and sutures (Bayford *et al* 2001, Fernández-Corazza *et al* 2017). Furthermore, a recently developed protocol employed EIT using injection patterns with one source and multiple sinks to generate an inhomogeneous conductivity map of the skull (Fernández-Corazza *et al* 2020). This novel method may enhance the current proposed EIT homogeneous model, to produce the most accurate heterogeneous representation of skull conductivity and thus reduce FP and IP errors further. Additional methodologies exist to determine individualised skull conductivities, such as those obtained with EEG and MEG (i.e. as in Gonçalves *et al* 2003a). Despite good characterisation of personalised skull conductivity using EIT, further research could employ these additional methods and determine differences between them and the impact of sutures and bone composition using these measurements.

4.3. Influence of age

The current findings employing age-appropriate conductivity values also indicate the importance of accounting for suture closure as a function of age for EEG source analysis. Specifically, the greatest FP-RE was shown across regions of high spongiform proportion, typically frontal regions, for all age-appropriate models. This error increased with increasing age, due to a higher relative difference between the EIT estimated global conductivity value and that of spongiform bone. Conversely, a greater error was revealed across areas of high compact bone for the 20 year old model, which is also supported by Azizollahi *et al* (2016) findings that skull conductivity affected EEG forward modelling in regions covered by cranial

bones. In line with Azizollahi *et al* (2016) and the current results, younger ages, particularly children with higher skull conductivities, may yield greater inaccuracies in regions of complete compact bone (typically temporal areas). Importantly, as discussed more thoroughly in section 4.1, accounting for suture closure, and thus differing conductivity, as a function of age further impacted EEG source analysis. These results outline not only the importance of including the sutures in EEG analysis, but also that accounting for their variation and fusion across the lifespan is imperative.

The relationship between skull conductivity and age, however, remains relatively unknown, with such a relationship being hypothesised from previous data in the current analysis. Future research should determine accurate and precise *in vivo* conductivity values as a function of age to assess the impact on EEG source analysis. Alongside this, the current volume conductor models assumed known and fixed non-skull tissue conductivity values. This also avoided unstable estimation and negative conductivities for EIT conductivity estimation. However, these tissues are equally subject to variation in the literature (McCann *et al* 2019), of which participant age, gender and measurement methodology may influence. Furthermore, skull and brain geometry, such as skull thickness and size, is also affected by participant age but was beyond the scope of the presented study, which utilised identical head geometries for all age-appropriate models. An important future avenue thus involves evaluating the influence that varying soft tissue conductivities has on EEG source estimation as well as including these unknown parameters for EIT skull and non-skull conductivity computation. Particularly imperative is including the changing head geometry as a function of participant age, alongside deviating conductivity values and ascertaining a more accurate representation of EEG forward and inverse computations when considering age-appropriate models.

4.4. Research and clinical applications

The source localisation errors from the current study are important for both research and clinical applications. Particularly in a clinical setting, head models are typically segmented using typical MRI procedures which are unable to accurately account for compact and spongiform layers or include the sutures (Fernández-Corazza *et al* 2017). Furthermore, suture closure cannot be obtained directly from CT and thus such deviation as a function of age has been omitted. As presented, this could yield source localisation errors between 2 and 4 cm, potentially crucial for resection and treatment purposes. For example, Aydin *et al* (2014) revealed source localisation inaccuracies of an approximately 1.5 cm radius for epileptic spikes when the skull was considered to have a global conductivity that approximated both compact

and spongiform layers into one compartment (compared to a model with distinction between the layers). This would greatly impact epilepsy resection surgeries. Further research, however, is imperative to explore real-world applications of neglecting the sutures, bone composition distribution, and aging skull conductivity. This can be done, for example, by utilising individualised, realistic, inhomogeneous skull conductivity models (as determined through high-quality CT and EIT acquisition) on evoked and event-related EEG data to further determine their clinical and research importance. Moreover, concurrent EEG and EIT methodologies can be employed in the future to non-invasively and cost-effectively obtain individualised and inhomogeneous conductivities (i.e. using the method proposed by Fernández-Corazza *et al* 2020) for such applications.

Our inverse solution calculations were also in a noiseless situation and therefore represent errors in the most optimum circumstances. In a more realistic setting, where noise (such as participant motion, physiological artifacts and environmental interference), is expected, these errors are hypothesised to increase. Similarly, real EIT data would incur artifacts due to participant movement, physiology and environmental factors, triggering potential inaccuracies in conductivity estimation (Lionheart 2004). For EEG source analysis, the effect of noise is supported by Montes-Restrapo *et al* (2014) where dipole estimation errors were considerably large for high levels of noise. Interestingly, the employed model accuracy was more important at lower levels of noise, where very noisy environments yielded similarly elevated errors across models. Understanding the influence of spatiotemporally correlated noise, for example incorporating spatiotemporally correlated Gaussian noise for both the EIT and EEG forward and inverse solutions is imperative for future research (Lionheart 2004, Beltrachini *et al* 2013).

5. Conclusion

The current study highlighted the importance skull conductivity deviation has on EEG forward solutions and source localisation. Omitting the presence of adult sutures incurred large EEG source analysis inaccuracies, up to 4.14 cm, directly beneath suture lines, particularly evident for dentate sutures. These inaccuracies remained even when suture closure and global conductivity variation as a function of age was accounted for, particularly from 20 to 50 years old. Furthermore, when neglecting changes in spongiform and marrow proportion across the skull, and thus assuming a homogeneous model, errors were reported up to 85% in the EEG-FP and 3.03 cm in the EEG-IP. Assuming higher homogeneous skull conductivity increased global error across areas of complete compact bone, such as temporal regions, whereas lower conductivity yielded greatest

miscalculations across high spongiform proportion, such as the frontal region. Estimating equivalent homogeneous conductivity from EIT reduced such errors. Future research is suggested to account for the presence of sutures and incorporate a heterogeneous model, as well as employ individualised *in vivo* conductivity values for the skull.

Data availability statement

The data that support the findings of this study are available upon reasonable request from the authors.

Acknowledgments

This work was supported by the Knowledge Economy Skills PhD Scholarship, Grant Number 512734. Knowledge Economy Skills Scholarships (KESS) is a pan-Wales higher level skills initiative led by Bangor University on behalf of the HE sector in Wales. It is part funded by the Welsh Government's European Social Fund (ESF) convergence programme for West Wales and the Valleys. This work was also partially funded by the Science and Technology Facilities Council, UK, through an Impact Acceleration Award.

Declarations of interest

None.

ORCID iDs

Hannah McCann  <https://orcid.org/0000-0002-3703-7996>

Leandro Beltrachini  <https://orcid.org/0000-0003-4602-1416>

References

- Acar Z A and Makeig S 2013 Effects of forward model errors on EEG source localization *Brain Topogr.* **26** 378–96
- Antonakakis M, Schrader S, Aydin Ü, Khan A, Gross J, Zervakis M, Rampp S and Wolters C H 2020 Inter-subject variability of skull conductivity and thickness in calibrated realistic head models *NeuroImage* **223** 117353
- Aubert-Broche B, Evans A C and Collins L 2006 A new improved version of the realistic digital brain phantom *NeuroImage* **32** 138–45
- Avery J, Dowrick T, Faulkner M, Goren N and Holder D 2017 A versatile and reproducible multi-frequency electrical impedance tomography system *Sensors* **17** 280
- Aydin Ü *et al* 2014 Combining EEG and MEG for the reconstruction of epileptic activity using a calibrated realistic volume conductor model *PLoS One* **9** e93154
- Azizollahi H, Aarabi A and Wallois F 2016 Effects of uncertainty in head tissue conductivity and complexity on EEG forward modeling in neonates *Hum. Brain Mapp.* **37** 3604–22
- Azizollahi H, Aarabi A and Wallois F 2020 Effect of structural complexities in head modeling on the accuracy of EEG source localization in neonates *J. Neural Eng.* **17** 056004
- Baillet S, Mosher J C and Leahy R M 2001 Electromagnetic brain mapping *IEEE Signal Process. Mag.* **18** 14–30
- Bayford R H, Gibson A, Tizzard A, Tidswell A T and Holder D S 2001 Solving the forward problem for the human head using

- IDEAS (integrated design engineering analysis software) a finite element modelling tool *Physiol. Meas.* **22** 55–63
- Beltrachini L 2019 The analytical subtraction approach for solving the forward problem in EEG *J. Neural Eng.* **16** 056029
- Beltrachini L, Von Ellenrieder N and Muravchik C H 2013 Shrinkage approach for spatiotemporal EEG covariance matrix estimation *IEEE Trans. Signal Process.* **61** 1797–808
- Bénar C G and Gotman J 2002 Modeling of post-surgical brain and skull defects in the EEG inverse problem with the boundary element method *Clin. Neurophysiol.* **113** 48–56
- Chen F, Hallez H and Staelens S 2010 Influence of skull conductivity perturbations on EEG dipole source analysis *Med. Phys.* **37** 4475–84
- Chiba F *et al* 2013 Age estimation by multidetector CT images of the sagittal suture *Int. J. Legal Med.* **127** 1005–11
- Dannhauer M, Lanfer B, Wolters C H and Knösche T R 2011 Modeling of the human skull in EEG source analysis *Hum. Brain Mapp.* **32** 1383–99
- Darbas M and Lohrengel S 2019 Review on mathematical modelling of electroencephalography (EEG) *Jahresbericht Dtsch. Mathematiker Vereinigung* **121** 3–39
- Fang Q and Boas D A 2009 Tetrahedral mesh generation from volumetric binary and grayscale images 2009 *IEEE Int. Symp. on Biomedical Imaging: From Nano to Macro* (IEEE) pp 1142–5
- Fernández-Corazza M, Beltrachini L, Von Ellenrieder N and Muravchik C H 2013 Analysis of parametric estimation of head tissue conductivities using electrical impedance tomography *Biomed. Signal Process. Control* **8** 830–7
- Fernández-Corazza M, Turovets S, Luu P, Price N, Muravchik C H and Tucker D 2017 Skull modeling effects in conductivity estimates using parametric electrical impedance tomography *IEEE Trans. Biomed. Eng.* **65** 1785–97
- Fernández-Corazza M, Turovets S and Muravchik C H 2020 A novel bounded EIT protocol to generate inhomogeneous skull conductivity maps non-invasively 2020 *42nd Annual Int. Conf. of the IEEE Engineering in Medicine & Biology Society (EMBC) (July)* (IEEE) pp 1440–3
- Fischl B 2012 FreeSurfer *NeuroImage* **62** 774–81
- Gençer N G and Acar C E 2004 Sensitivity of EEG and MEG measurements to tissue conductivity *Phys. Med. Biol.* **49** 701
- Gonçalves S, De Munck J C, Heethaar R M, Da Silva F L and Van Dijk B W 2000 The application of electrical impedance tomography to reduce systematic errors in the EEG inverse problem—a simulation study *Physiol. Meas.* **21** 379
- Gonçalves S, de Munck J C, Verbunt J P, Heethaar R M and Da Silva F H L 2003a *In vivo* measurement of the brain and skull resistivities using an EIT-based method and the combined analysis of SEF/SEP data *IEEE Trans. Biomed. Eng.* **50** 1124–7
- Gonçalves S I, de Munck J C, Verbunt J P, Bijma F, Heethaar R M and Da Silva F L 2003b *In vivo* measurement of the brain and skull resistivities using an EIT-based method and realistic models for the head *IEEE Trans. Biomed. Eng.* **50** 754–67
- Gray H 1878 *Anatomy of the Human Body* vol 8 (Pennsylvania: Lea & Febiger)
- Grech R, Cassar T, Muscat J, Camilleri K P, Fabri S G, Zervakis M, Xanthopoulos P, Sakkalis V and Vanrumste B 2008 Review on solving the inverse problem in EEG source analysis *J. Neuroeng. Rehabil.* **5** 1–33
- Hauelsen J, Büttner A, Nowak H, Brauer H and Weiller C 1999 The influence of conductivity changes in boundary element compartments on the forward and inverse problem in electroencephalography and magnetoencephalography *Biomed. Eng.* **44** 150–7
- Henry J C 2006 Electroencephalography: basic principles, clinical applications, and related fields *Neurology* **67** 2092
- Holder D S 1992 Electrical impedance tomography (EIT) of brain function *Brain Topogr.* **5** 87–93
- Ibáñez A *et al* 2011 Cortical deficits of emotional face processing in adults with ADHD: its relation to social cognition and executive function *Soc. Neurosci.* **6** 464–81
- Idriz S, Patel J H, Ameli Renani S, Allan R and Vlahos I 2015 CT of normal developmental and variant anatomy of the pediatric skull: distinguishing trauma from normality *Radiographics* **35** 1585–601
- Jangietriew B, Thamtakerngkit S, Wongchanapai W and Sangvichien S 2007 Cranial suture closure and age determination in the thai population *Siriraj Med. J.* **59** 226–31 (available at: <https://he02.tci-thaijo.org/index.php/sirirajmedj/article/view/246137>)
- Khan S, Manwaring P, Borsic A and Halter R 2014 FPGAs-based voltage and current dual drive system for high frame rate electrical impedance tomography *IEEE Trans. Med. Imaging* **34** 888–901
- Kumar A, Ghosh S K and Pareek V 2018 Establishing identity from the skeletal remains: in reference of Alum Bheg a martyr from 1857 Indian freedom struggle *Pre-prints*
- Lanfer B, Scherg M, Dannhauer M, Knösche T R, Burger M and Wolters C H 2012 Influences of skull segmentation inaccuracies on EEG source analysis *NeuroImage* **62** 418–31
- Law S K 1993 Thickness and resistivity variations over the upper surface of the human skull *Brain Topogr.* **6** 99–109
- Lew S, Sliva D D, Choe M S, Grant P E, Okada Y, Wolters C H and Hämäläinen M S 2013 Effects of sutures and fontanelles on MEG and EEG source analysis in a realistic infant head model *NeuroImage* **76** 282–93
- Lionheart W R 2004 EIT reconstruction algorithms: pitfalls, challenges and recent developments *Physiol. Meas.* **25** 125
- Lipsett B J, Reddy V and Steanson K 2019 Anatomy, head and neck, fontanelles
- Mamatjan Y, Ahn S, Oh T and Adler A 2012 Optimized electrode positions and stimulation patterns in head EIT *CMBES Proc.* **35** 23
- McCann H, Ahsan S T, Davidson J L, Robinson R L, Wright P and Pomfret C J 2011 A portable instrument for high-speed brain function imaging: FEITER 2011 *Annual Int. Conf. of the IEEE Engineering in Medicine and Biology Society (August)* (IEEE) pp 7029–32
- McCann H, Pisano G and Beltrachini L 2019 Variation in reported human head tissue electrical conductivity values *Brain Topogr.* **32** 825–58
- McCann H M and Beltrachini L 2021 Does participant's age impact on tDCS induced fields? Insights from computational simulations *Biomed. Phys. Eng. Express* **7** 045018
- Michel C M, Murray M M, Lantz G, Gonzalez S, Spinelli L and de Peralta R G 2004 EEG source imaging *Clin. Neurophysiol.* **115** 2195–222
- Miura T, Perlyn C A, Kinboshi M, Ogihara N, Kobayashi-Miura M, Morriss-Kay G M and Shiota K 2009 Mechanism of skull suture maintenance and interdigitation *J. Anat.* **215** 642–55
- Montes V, Hallez H and Staelens S 2011 Influence of skull inhomogeneities on EEG source localization 2011 *8th Int. Symp. on Noninvasive Functional Source Imaging of the Brain and Heart and the 2011 8th Int. Conf. on Bioelectromagnetism* (IEEE) pp 72–76
- Montes-Restrepo V, van Mierlo P, Strobbe G, Staelens S, Vandenberghe S and Hallez H 2014 Influence of skull modeling approaches on EEG source localization *Brain Topogr.* **27** 95–111
- Nakahara K, Utsuki S, Shimizu S, Iida H, Miyasaka Y, Takagi H, Oka H and Fujii K 2006 Age dependence of fusion of primary occipital sutures: a radiographic study *Child's Nervous Syst.* **22** 1457–9
- Oh T, Gilad O, Ghosh A, Schuettler M and Holder D S 2011 A novel method for recording neuronal depolarization with recording at 125–825 Hz: implications for imaging fast neural activity in the brain with electrical impedance tomography *Med. Biol. Eng. Comput.* **49** 593–604
- Oostenveld R, Fries P, Maris E and Schoffelen J-M 2011 FieldTrip: open source software for advanced analysis of MEG, EEG, and invasive electrophysiological data *Comput. Intell. Neurosci.* **2011** 1–9

- Pascual-Marqui R D 2002 Standardized low-resolution brain electromagnetic tomography (sLORETA): technical details *Methods Find Exp. Clin. Pharmacol.* **24** 5–12 (PMID: 12575463) (available at: <https://pubmed.ncbi.nlm.nih.gov/12575463/>)
- Ruengdit S, Case D T and Mahakkanukrauh P 2020 Cranial suture closure as an age indicator: a review *Forensic Sci. Int.* **307** 110111
- Russell W P and Russell M R 2018 Anatomy, head and neck, coronal suture, 26 September 2018 (Treasure Island, FL: StatPearls Publishing) (PMID: 30252267)
- Sadleir R J and Argibay A 2007 Modeling skull electrical properties *Ann. Biomed. Eng.* **35** 1699–712
- Singh P, Oberoi S S, Gorea R K and Kapila A K 2004 Age estimation in old individuals by CT scan of skull *JIAFM* **26** 0971–3
- Tadel F, Baillet S, Mosher J C, Pantazis D and Leahy R M 2011 Brainstorm: a user-friendly application for MEG/EEG analysis *Comput. Intell. Neurosci.* **2011** 879716
- Tang C, You F, Cheng G, Gao D, Fu F, Yang G and Dong X 2008 Correlation between structure and resistivity variations of the live human skull *IEEE Trans. Biomed. Eng.* **55** 2286–92
- Todd T W and Lyon D W 1925 Cranial suture closure *Am. J. Phys. Anthropol.* **8** 23
- Torquato S and Hyun S 2001 Effective-medium approximation for composite media: realizable single-scale dispersions *J. Appl. Phys.* **89** 1725–9
- Valdés-Hernández P A, Von Ellenrieder N, Ojeda-Gonzalez A, Kochen S, Alemán-Gómez Y, Muravchik C and Valdés-Sosa P A 2009 Approximate average head models for EEG source imaging *J. Neurosci. Methods* **185** 125–32
- Vallaghé S and Clerc M 2008 A global sensitivity analysis of three-and four-layer EEG conductivity models *IEEE Trans. Biomed. Eng.* **56** 988–95
- Vanrumste B, Van Hoey G, Van de Walle R, D'havé M, Lemahieu I and Boon P 2000 Dipole location errors in electroencephalogram source analysis due to volume conductor model errors *Med. Biol. Eng. Comput.* **38** 528–34
- Von Ellenrieder N, Beltrachini L, Muravchik C H and Gotman J 2014 Extent of cortical generators visible on the scalp: effect of a subdural grid *NeuroImage* **101** 787–95
- Vorwerk J, Aydin Ü, Wolters C H and Butson C R 2019 Influence of head tissue conductivity uncertainties on EEG dipole reconstruction *Front. Neurosci.* **13** 531
- Vorwerk J, Cho J-H, Rampp S, Hamer H, Knösche T R and Wolters C H 2014 A guideline for head volume conductor modeling in EEG and MEG *NeuroImage* **100** 590–607
- Vorwerk J, Clerc M, Burger M and Wolters C H 2012 Comparison of boundary element and finite element approaches to the EEG forward problem *Biomed. Eng.* **57** 795–8
- Vu H L, Panchal J, Parker E E, Levine N S and Francel P 2001 The timing of physiologic closure of the metopic suture: a review of 159 patients using reconstructed 3D CT scans of the craniofacial region *J. Craniofac. Surg.* **12** 527–32
- Wolters C H, Anwander A, Tricoche X, Weinstein D, Koch M A and Macleod R S 2006 Influence of tissue conductivity anisotropy on EEG/MEG field and return current computation in a realistic head model: a simulation and visualization study using high-resolution finite element modeling *NeuroImage* **30** 813–26